*Structural Engineering and Mechanics, Vol. 42, No. 6 (2012) 883-897*
DOI: http://dx.doi.org/10.12989/sem.2012.42.6.883


# Yield line mechanism analysis of cold-formed channel sections with edge stiffeners under bending

S. Maduliat*[1], M.R. Bambach[2] and X.L. Zhao[1]

[1]*Department of Civil Engineering, Monash University, Clayton Campus, VIC 3800, Australia*
[2]*IRMRC, Faculty of Science, University of New South Wales, NSW 2052, Australia*

*(Received November 21, 2011, Revised May 2, 2012, Accepted May 17, 2012)*

**Abstract.** Cold-formed channel sections are used in a variety of applications in which they are required to absorb deformation energy. This paper investigates the collapse behaviour and energy absorption capability of cold-formed steel channels with flange edge stiffeners under large deformation major-axis bending. The Yield Line Mechanism technique is applied using the energy method, and based upon measured spatial plastic collapse mechanisms from experiments. Analytical solutions for the collapse curve and in-plane rotation capacity are developed, and used to model the large deformation behaviour and energy absorption. The analytical results are shown to compare well with experimental values. Due to the complexities of the yield line model of the collapse mechanism, a simplified procedure to calculate the energy absorbed by channel sections under large bending deformation is developed and also shown to compare well with the experiments.

**Keywords:** cold-formed steel; channels; yield line mechanisms; major-axis bending; energy absorption

## 1. Introduction

Cold-formed sections have been used as structural elements in building systems, car bodies, aircraft and highway barriers. They may be required to dissipate energy during plastic collapse, or when subjected to seismic or dynamic loads. They are primarily made from thin-walled sections due to these sections being efficient and versatile (Nagel 2005). When thin-walled sections fail in bending, they undergo plastic folding of the cross-sections walls and collapse in a spatial plastic mechanism. Yield Line Mechanism (YLM) analysis of the collapse mechanism provides a bending moment-rotation relationship, from which estimates of member strengths and energy absorption capacity can be estimated.

Davies *et al*. (1975) analysed a plate element under uniaxial compression and proposed a yield line theory. They showed that the ultimate load capacity of the plate depends on the localised yielded portion of the plate. Murray (1984) proposed a yield line theory with ignoring the shear force and twisting moment. Zhao and Hancock (1993) performed experimental tests on plastic hinges under axial force for different inclination angles. They compared their test with the theory results of Murray (1984) and also the Zhao and Hancock (1993a) theory results. They concluded

*Corresponding author, Ph.D., E-mail: smaduliat@hotmail.com

that Murray's theory, due to not including the shear force and twisting moment, miscalculates the plastic moment drop.

The first step of such an analysis is to correctly identify the spatial plastic mechanism that forms in the member, for which experimental observations have been found to be the most reliable method. Based on experimental observations, Murray and Khoo (1981) developed eight basic mechanisms for plates and five combinations of simple mechanisms for channel columns. Kecman (1983) studied the bending collapse behaviour of rectangular and square hollow sections, and developed a yield line mechanism model including travelling yield lines. Kecman's model was verified using experimental results from fifty six bending tests on twenty seven different sections. Kotelko (1996) investigated yield line mechanisms of rectangular and trapezoidal box section beams with a high width to depth ratio compared to Kecman's sections. Kotelko's models are similar to Kecman's, with a slight difference of the web hinge line angles. Kotelko (2007) subsequently developed mechanism models for channel and hat-sections in compression. By using YLM, Setiyono (2007) estimated the ultimate capacity of a cold-formed channel section under axial compression load. Setiyono assessment indicated that the YLM results are in a good agreement with the test results. Elchalakani (2007) found a good agreement between the measured and predicted collapse curve using YLM. As the inclination angle and the number of inclined yield lines in the local plastic mechanism have a considerable influence on the final analysis results, Zhao (2003) and Ungureanu *et al*. (2010) collected basic yield line mechanisms from a number of authors. This work presents a comprehensive review of YLM analysis and its application to steel structures and connections.

In the present paper the YLM analysis approach is applied to cold-formed steel channel sections subjected to major-axis pure bending, where the channel flanges have simple edge stiffeners or complex edge stiffeners. The mechanisms are based on the experimental results of a broad range of channel sections, and the plastic collapse curves developed from the analysis are shown to compare well with the experimental curves. Similar to Ye *et al*. (2007) study, a semi-empirical solution for the collapse curve is then developed, in order to simplify the complex calculation of the exact curve. The collapse curve solutions are then used in conjunction with elastic and in-plane plastic theory, to fully describe the large deformation bending moment-rotation behaviour of the channel sections, which allows for the total energy absorbed to be calculated analytically. The energy absorption results are shown to compare well with the experimental values, and provide analysts with a robust tool for estimating the energy absorption capacity of cold-formed channel sections in pure bending.

## 2. Development of the YLM model for channel sections with edge stiffeners

### *2.1 Spatial plastic mechanism from experimental results*

To define the spatial plastic mechanism for the YLM analysis, experimental observations of 40 channel sections cold-formed from G450 grade steel of nominal thickness 1.6 mm under major-axis bending were employed. The flanges of the channel sections contained either a single lip edge stiffener (simple stiffeners), or two lip edge stiffeners (complex stiffeners). The measured section dimensions are shown in Table 1, as are the slenderness ratios, elastic slenderness limits and plastic slenderness limits calculated according to the Australian Standard for steel structures AS4100

Table 1 Section properties and section slenderness (Eq. (53)) and slenderness limits according to AS4100 (1998)

| Sections | Thickness | | | | | | | |
|---|---|---|---|---|---|---|---|---|
| | $b_4$ (mm) | $b_3$ (mm) | $b_2$ (mm) | $b_1$ (mm) | $t$ (mm) | $\lambda_s$ | $\lambda_{sy}$ | $\lambda_{sp}$ |
| 3 | 12.32 | 15.94 | 44.92 | 122.14 | 1.57 | 36.06 | 35 | 8 |
| 4 | 14.20 | 14.94 | 62.75 | 79.85 | 1.56 | 54.06 | 35 | 8 |
| 5 | 12.62 | 21.67 | 41.49 | 111.16 | 1.57 | 32.88 | 35 | 8 |
| 6 | 12.51 | 16.29 | 41.27 | 129.03 | 1.57 | 113.99 | 110 | 22 |
| 7 | 12.39 | 15.78 | 34.99 | 139.88 | 1.58 | 123.26 | 110 | 22 |
| 8 | 11.82 | 17.66 | 48.23 | 110.04 | 1.59 | 38.64 | 35 | 8 |
| 9 | 9.78 | 18.06 | 56.65 | 99.00 | 1.56 | 48.25 | 35 | 8 |
| 10 | 17.12 | 17.98 | 49.36 | 99.83 | 1.54 | 41.42 | 35 | 8 |
| 11 | 10.85 | 16.19 | 60.10 | 94.21 | 1.54 | 52.20 | 35 | 8 |
| 12 | 10.85 | 16.50 | 50.93 | 113.76 | 1.53 | 43.20 | 35 | 8 |
| 13 | 9.98 | 14.27 | 58.18 | 102.90 | 1.57 | 48.89 | 35 | 8 |
| 14 | | 22.74 | 47.59 | 121.10 | 1.58 | 38.78 | 35 | 8 |
| 15 | | 13.34 | 42.49 | 141.02 | 1.58 | 125.88 | 110 | 22 |
| 16 | | 18.67 | 31.40 | 159.19 | 1.57 | 143.73 | 110 | 22 |
| 17 | | 12.44 | 37.01 | 161.69 | 1.54 | 148.93 | 110 | 22 |
| 18 | | 17.34 | 62.09 | 102.68 | 1.56 | 52.89 | 35 | 8 |
| 19 | | 12.45 | 47.50 | 141.42 | 1.55 | 128.70 | 110 | 22 |
| 20 | | 14.53 | 55.88 | 121.20 | 1.56 | 47.10 | 35 | 8 |
| 21 | | 12.88 | 65.86 | 103.61 | 1.57 | 56.09 | 35 | 8 |
| 22 | | 20.00 | 39.99 | 89.00 | 1.50 | 33.34 | 35 | 8 |
| 23 | | 19.96 | 45.00 | 89.98 | 1.50 | 38.25 | 35 | 8 |
| 24 | | 19.96 | 49.99 | 89.96 | 1.50 | 43.15 | 35 | 8 |
| 25 | | 19.97 | 35.00 | 79.80 | 1.55 | 27.53 | 35 | 8 |
| 26 | | 20.00 | 40.20 | 79.99 | 1.50 | 33.54 | 35 | 8 |
| 27 | | 19.97 | 45.00 | 79.98 | 1.52 | 37.75 | 35 | 8 |
| 28 | | 19.96 | 29.97 | 70.05 | 1.50 | 23.51 | 35 | 8 |
| 29 | | 19.95 | 34.99 | 70.10 | 1.55 | 27.52 | 35 | 8 |
| 30 | | 19.99 | 39.97 | 70.00 | 1.50 | 33.32 | 35 | 8 |
| 31 | | 20.00 | 25.00 | 58.90 | 1.50 | 18.64 | 35 | 8 |
| 32 | | 19.97 | 29.96 | 60.80 | 1.55 | 22.74 | 35 | 8 |
| 33 | | 19.97 | 35.00 | 60.40 | 1.55 | 27.53 | 35 | 8 |
| 34 | | 14.80 | 19.90 | 49.50 | 1.55 | 13.19 | 35 | 8 |
| 35 | | 14.96 | 24.99 | 50.10 | 1.50 | 18.63 | 35 | 8 |
| 36 | | 14.95 | 29.97 | 50.10 | 1.50 | 23.51 | 35 | 8 |
| 37 | | 9.75 | 14.78 | 38.20 | 1.55 | 30.56 | 110 | 22 |
| 38 | | 9.63 | 19.75 | 39.40 | 1.55 | 13.05 | 35 | 8 |
| 39 | | 9.83 | 24.68 | 38.50 | 1.55 | 17.73 | 35 | 8 |
| 40 | | 9.20 | 10.45 | 28.10 | 1.55 | 20.98 | 110 | 22 |
| 41 | | 9.70 | 14.50 | 29.50 | 1.55 | 8.07 | 35 | 8 |
| 42 | | 9.73 | 19.55 | 29.00 | 1.55 | 12.86 | 35 | 8 |

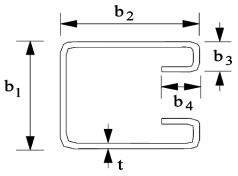

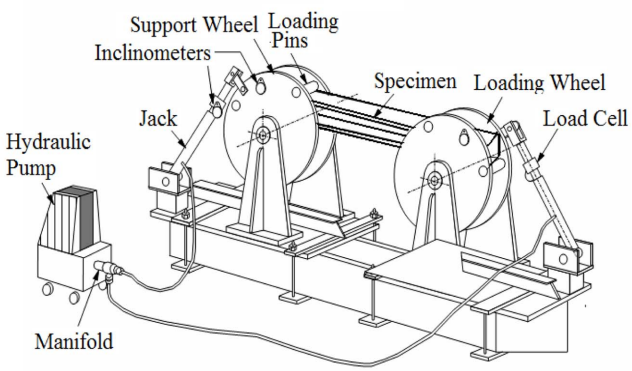


Fig. 1 Schematic of the Monash pure bending rig

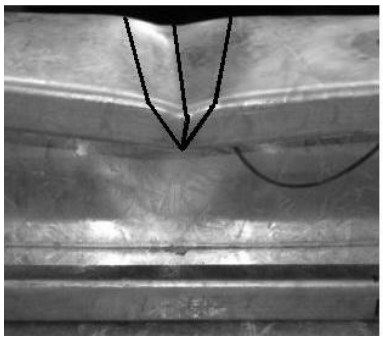

Fig. 2 Typical observed YLM model for the flange and lip edge stiffener

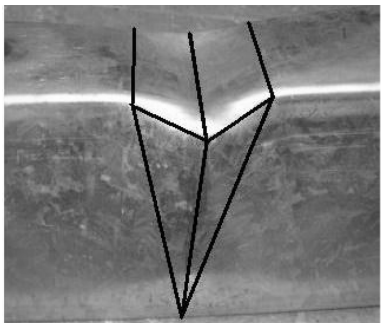

Fig. 3 Typcial observed YLM model for the web and the flange

(1998). The channel sections were tested using a large deformation pure bending rig developed by Cimpoeru (1992), as shown in Fig. 1. Fig. 2 shows the typical experimental collapse mechanisms for the flange and edge stiffeners, and Fig. 3 for the webs of the channel sections. Full details of the experimental setup and results are presented in Maduliat *et al.* (2012).

### 2.2 Analytical solution for the collapse curve

The energy method is used in the present analysis to establish the plastic collapse curves, whereby the equilibrium condition is derived by equating the work of external loads to the work absorbed by the mechanism during a kinematically admissible displacement, and is applied to stationary yield lines. The total work absorbed by the collapse mechanism is the sum of the work absorbed by all the yield lines in the mechanism

$$W(\theta) = \sum_{1}^{n} W_i(\theta) \tag{1}$$

where $n$ is the number of yield lines in the model.

The bending moment is obtained from Eq. (2)

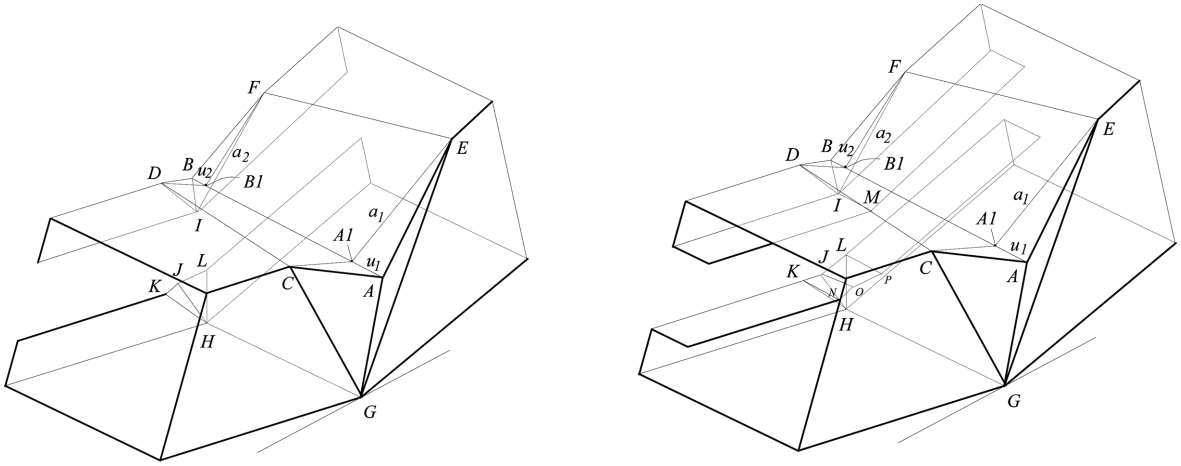


(a) Simple lip edge stiffener (b) Complex lip edge stiffener

Fig. 4 YLM model for cold-formed channel sections with flange edge stiffeners

$$M(\theta) = \frac{dW}{d\theta} \tag{2}$$

where $\theta$ is the rotational angle of the beam. Therefore, for different values of rotation angle the bending moment can be determined, and the collapse curve (moment-rotation graph) can be incrementally plotted.

The plastic mechanism that forms in the compression flange in Fig. 2 is similar to those found by Kecman (1983), and the work components developed by Kecman for the energy absorption of such yield lines are adopted for the compression flange hinges in the present channel sections. Similarly, the V-shape mechanism in the web exemplified in Fig. 3 is similar to that proposed by Kotelko (2007), and Kotelko's work components are adopted for the webs. Additional work components are introduced for the yield lines in the simple and complex edge stiffeners, and the tension flanges. The YLM model thus developed for the cold-formed channel sections with simple and complex lip edge stiffeners are shown in Fig. 4, and the work components for each yield line are defined as follows

$$W_1 = W_{EF} + W_{CD} = \frac{m_p b_2(\gamma_1 + \gamma_2)}{\cos\alpha} \tag{3}$$

$$\alpha = \arctan\left(\frac{a_1 - a_2}{b_2}\right) \tag{4}$$

$$\gamma_1 + \theta = \arccos\left(\frac{(a_1 - b_1\tan\theta)\cos\theta}{a_1}\right) \tag{5}$$

$$\gamma_2 + \theta = \arccos\left(\frac{(a_2 - b_3\tan\theta)\cos\theta}{a_2}\right) \tag{6}$$

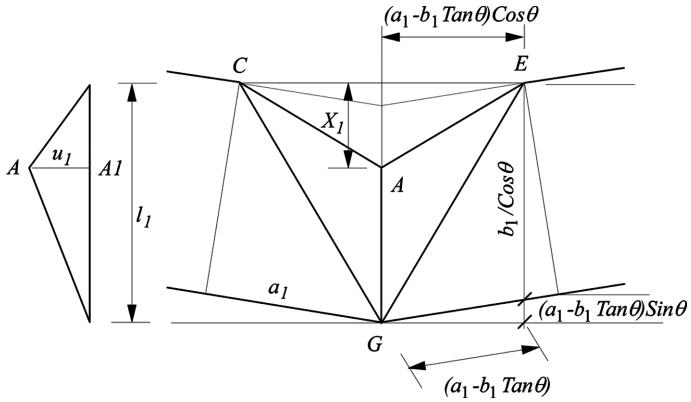


Fig. 5 Longitudinal cross-section of the web YLM model

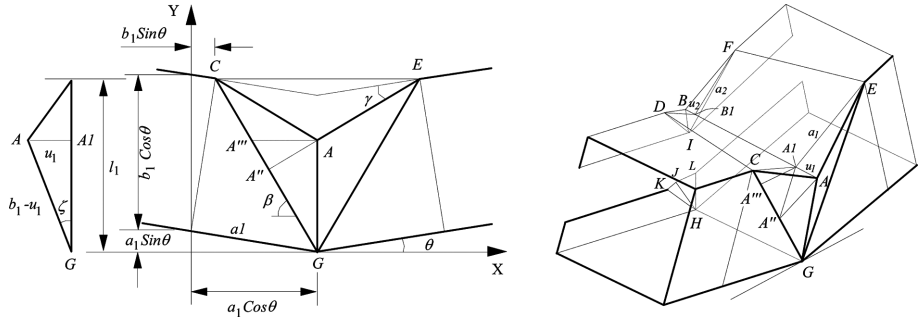


Fig. 6 The angle between plane *GCA* and plane $GCA_1$

$$X_1 = \sqrt{a_1^2 - ((a_1 - b_1\tan\theta)\cos\theta)^2} \tag{7}$$

$$l_1 = \left(\frac{b_1}{\cos\theta} + (a_1 - b_1\tan\theta)\sin\theta\right) - X_1 \tag{8}$$

$$u_1^2 = (b_1 - u_1)^2 - l_1^2 \Rightarrow u_1 = \frac{b_1^2 - l_1^2}{2b_1} \tag{9}$$

$$\xi_1 = \arcsin\left(\frac{u_1}{b_1 - u_1}\right), \quad \xi_2 = \arcsin\left(\frac{u_2}{b_3 - u_2}\right) \tag{10}$$

$$W_2 = W_{AB} = m_p(b_2 + u_1 + u_2)(\gamma_1 + \gamma_2) \tag{11}$$

$$W_3 = W_{A1E} + W_{A1E} = 2m_p a_1 \frac{\pi}{2} \tag{12}$$

$$W_4 = W_{B1F} + W_{B1D} = 2m_p a_2 \frac{\pi}{2} \tag{13}$$

$$W_5 = W_{GC} + W_{GE} = 2m_p \eta_1 l_{CG} \tag{14}$$

where the angles and dimensions are shown in Figs. 5 and 6.

The $(x,y,z)$ co-ordinates of points $G$, $C$ and $A_1$ (Fig. 6) are as follows, where $z$ is into the page

$$G:(a_1\cos\theta, 0, 0) \quad C:(b_1\cos\theta, b_1\cos\theta, a_1\sin\theta, 0) \quad A_1:(a_1\cos\theta, (b_1-u_1)\cos\xi_1, 0) \tag{15}$$

The slope of $CG$ is

$$\tan\beta_1 = ABS\left(\frac{y_C-y_G}{x_C-x_G}\right) \tag{16}$$

The $(x,y,z)$ co-ordinates of $A'''$ are

$$x_{A'''} = x_C+\frac{y_C-y_{A_1}}{\tan\beta_1}$$
$$y_{A'''} = y_{A_1}$$
$$z_{A'''} = 0 \tag{17}$$

The angle $\eta_1$ is the angle between plane $GCA_1$ and plane $GCA$, and the lengths of $A_1A'''$ and $A_1A''$ are

$$l_{A_1A'''} = \sqrt{((x_{A_1}-x_{A'''})^2+(y_{A_1}-y_{A'''})^2+(z_{A_1}-z_{A'''})^2)} \tag{18}$$

$$l_{A_1A''} = l_{A_1A'''}\sin\beta_1 \tag{19}$$

$$\eta_1 = \arctan\left(\frac{u_1}{l_{A_1A''}}\right) \tag{20}$$

$$l_{CG} = \sqrt{(b_1^2+a_1^2)} \tag{21}$$

$$W_6 = W_{ID}+W_{IF} = 2m_p\eta_2 l_{ID} \tag{22}$$

The $(x,y,z)$ co-ordinates of points $I$, $D$ and $B_1$ (Fig. 6) are as follows, where $z$ is into the page

$$I:(a_2\cos\theta, 0, 0) \quad D:(b_3\sin\theta, b_3\cos\theta+a_2\sin\theta, 0) \quad B_1:(a_2\cos\theta, (b_3-u_2)\cos\xi_2, 0) \tag{23}$$

The slope of $ID$ is

$$\tan\beta_2 = ABS\left(\frac{y_D-y_I}{x_D-x_I}\right) \tag{24}$$

The $(x,y,z)$ co-ordinates of $B'''$ are

$$x_{B'''} = x_D+\frac{y_D-y_{B_1}}{\tan\beta_2}$$
$$y_{B'''} = y_{B_1}$$
$$z_{B'''} = 0 \tag{25}$$

The angle $\eta_2$ is the angle between plane $IDB_1$ and plane $IDB$, and the lengths $B_1B'''$ and $B_1B''$

and remaining work components are

$$l_{B_1B'''} = \sqrt{((x_{B_1} - x_{B'''})^2 + (y_{B_1} - y_{B'''})^2 + (z_{B_1} - z_{B'''})^2)} \tag{26}$$

$$l_{B_1B''} = l_{B_1B'''} \sin\beta_2 \tag{27}$$

$$\eta_2 = \arctan\left(\frac{u_2}{l_{B_1B''}}\right) \tag{28}$$

$$l_{DI} = \sqrt{(b_3^2 + a_2^2)} \tag{29}$$

$$W_7 = W_{GA} = \int_0^{l_{GA}} m_p \frac{l_r}{r_{GA}} dl_G \tag{30}$$

$$l_r = \frac{l_G}{l_{GA}} u_1 \& r_{GA} = \frac{l_{GA}}{l_G} r_1 \tag{31}$$

$$W_{GA} = \int_0^{l_{GA}} m_p \frac{l_G^2 u_1}{r_1 l_{GA}^2} dl_G = \frac{m_p u_1}{r_1 l_{GA}^2} \left[\frac{l_G^3}{3}\right]_0^{l_{GA}} \tag{32}$$

$$W_{GA} = \frac{m_p u_1 l_{GA}}{3 r_1} \tag{33}$$

$$W_8 = W_{IB} = \int_0^{l_{IB}} m_p \frac{l_r}{r_{IB}} dl_L \tag{34}$$

$$l_r = \frac{l_I}{l_{IB}} u_2 \& r_{IB} = \frac{l_{IB}}{l_I} r_2 \tag{35}$$

$$W_{IB} = \int_0^{l_{IB}} m_p \frac{l_I^2 u_2}{r_2 l_{IB}^2} dl_I = \frac{m_p u_2}{r_2 l_{IB}^2} \left[\frac{l_I^3}{3}\right]_0^{l_{IB}} \tag{36}$$

$$W_{IB} = \frac{m_p u_2 l_{IB}}{3 r_2} \tag{37}$$

$$r_1 = \left(0.07 - \frac{\theta}{70}\right) a_1 \tag{38}$$

$$r_2 = \left(0.07 - \frac{\theta}{70}\right) a_2 \tag{39}$$

$$W_9 = W_{AC} + W_{AE} = 2A_{ACA_1} \frac{m_p}{r_1} \tag{40}$$

$$A_{ACA_1} = \frac{u_1 a_1}{2} \tag{41}$$

$$W_{10} = W_{BD} + W_{BF} = 2A_{BDB_1}\frac{m_p}{r_2} \tag{42}$$

$$A_{BDB_1} = \frac{u_2 a_2}{2} \tag{43}$$

$$W_{11} = W_{GH} = 2m_p b_2 \theta \tag{44}$$

$$W_{12} = W_{HK} + W_{HL} = W_{ID} + W_{IF} \tag{45}$$

$$W_{13} = W_{HJ} = W_{IB}\left(\frac{l_{HJ}}{l_{IB}}\right) \tag{46}$$

$$W_{14} = W_{IM} = 2m_p b_4 \theta \tag{47}$$

$$W_{15} = W_{KN} + W_{JO} + W_{LP} = 2m_p b_4 \gamma_2 + 2m_p b_4 \gamma_2 \tag{48}$$

where $m_p$ is the plastic moment capacity of the steel sheet

$$m_p = \frac{F_y t^2}{4} \tag{49}$$

It is noted that the dimension $a_1$ took the assumed value of the minimum of 1/3 of the web depth and 1/3 of the flange width, and $a_2$ took the assumed value of the minimum of 1/3 of the edge stiffener depth and 1/3 of the flange width (Fig. 4). These assumed values closely resembled the measured experimental values, and simplified the calculations.

### 2.3 Analytical solution for the rotation capacity

The rotation capacity ($R$) is a measure of the extent to which a section may maintain in-plane yielding prior to collapsing in a plastic mechanism. In accordance with the technique developed for thin-walled hat-sections in bending by Bambach *et al*. (2009), using Tan (2009) test results, it is assumed that the rotation capacity varies from one to four for non-compact sections and exceeds four for compact sections, and that the value is a function of the section slenderness ($\lambda_s$). Using the present experimental results an empirical equation for determining the rotation capacity of a channel section from its slenderness value was generated. The following equations are proposed for determining the rotation capacity of cold-formed channel sections in pure major-axis bending

$$\lambda_s \le \lambda_p, \quad R = \left(\frac{\lambda_p}{\lambda_s}\right)4 \quad \text{at} \quad M_p \tag{50}$$

$$\lambda_p < \lambda_s \le \lambda_y, \quad R = \left(\frac{\lambda_y - \lambda_s}{\lambda_y - \lambda_p}\right)4 \quad \text{at} \quad M_y \tag{51}$$

$$\lambda_y < \lambda_s, \qquad R = 0 \tag{52}$$

where $\lambda_s$ is the value of either the web or flange slenderness ratio with the greatest value of $\lambda_e/\lambda_{ey}$, $\lambda_y$ (elastic slenderness limit) and $\lambda_p$ (plastic slenderness limit) respectively are taken as the values of the web or flange element slenderness limits, $\lambda_{ey}$ and $\lambda_{ep}$, given in AS4100 (1998) for the element

of the cross-section which has the greatest value of $\lambda_e/\lambda_{ey}$, and the slenderness ratio of each element ($\lambda_e$) is calculated according to Eq. (53)

$$\lambda_e = \left(\frac{b}{t}\right)\sqrt{\frac{f_y}{250}} \tag{53}$$

where $t$ is the element thickness and $b$ is the clear width of the element between the face of supporting elements.

Accordingly, the bending moment is assumed to maintain the plastic moment for compact sections (Eq. (50)), the yield moment for non-compact sections (Eq. (51)), for the rotation capacity defined in Eqs. (50) and (51). Consequently, the plastic collapse curve is shifted in order to begin at the curvature that corresponds to the end of the in-plane plastic stage defined by $R$. For slender sections where $R = 0$ (Eq. (52)), the plastic collapse curve is assumed to begin at the curvature that corresponds to the ultimate moment capacity. The theoretical ultimate moment capacities of the channel sections were calculated according to AS4100 (1998). For all section classes, the sections are assumed to respond in a linear-elastic manner prior to reaching the ultimate moment capacity. Sample large deformation bending solutions for slender, non-compact and compact sections are shown in Fig. 7. The values of $R$ calculated with Eqs. (50) to (52) are compared with the experimentally determined values in Table 2, where they are shown to provide reasonable predictions, and on average are 33% conservative.

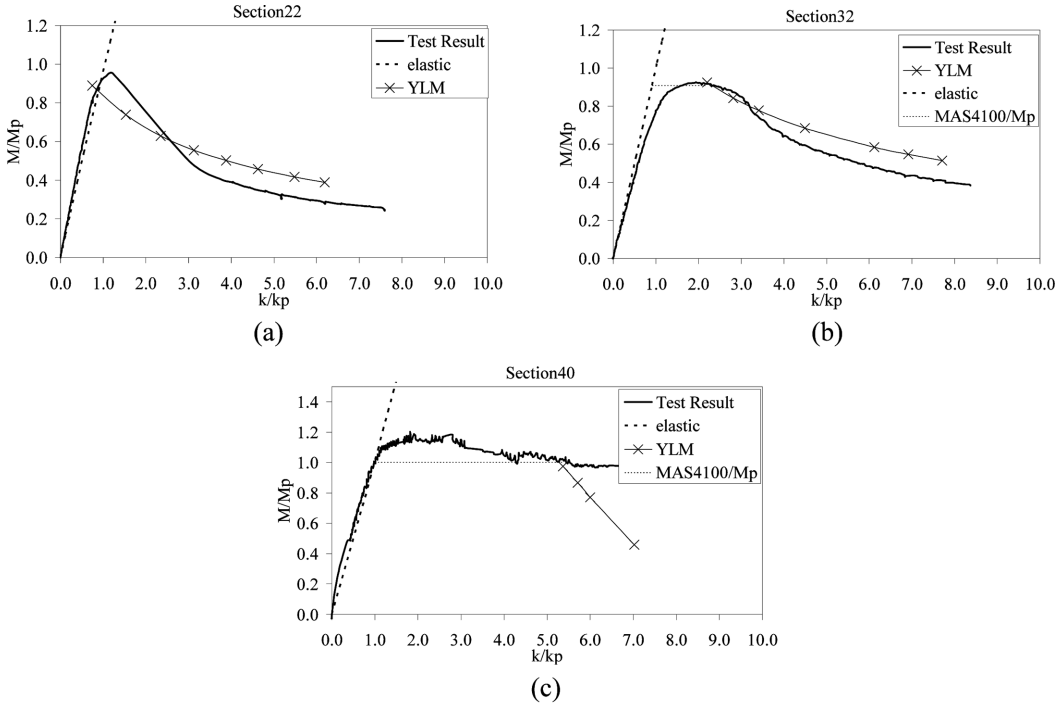


Fig. 7 Sample normalised moment-curvature diagrams from the experiments compared with the YLM results for: (a) slender, (b) non-compact and (c) compact sections

Table 2 Calculated rotation capacity value, energy absorption and constant $X$

| Sections | Calculated | | Test | Absorbed Energy | Best fit with test graph | | Absorbed Energy |
|---|---|---|---|---|---|---|---|
| | R | | R | (test/YLM) | $M/Mp=X(k/kp)^{-.665}$ $X$ | $X=2.8(\lambda_s/\lambda_{sp})^{-.665}$ | (test/Simple method) |
| 3 | 0.00 | | 0.4 at My | 1.08 | 1.00 | 1.03 | 1.10 |
| 4 | 0.00 | | 0.00 | 1.01 | 0.75 | 0.79 | 0.93 |
| 5 | 0.31 | at My | 0.80 at My | 0.9 | 1.00 | 1.09 | 0.83 |
| 6 | 0.00 | | 0.20 at My | 0.84 | 1.00 | 0.94 | 0.96 |
| 7 | 0.00 | | 0.60 at My | **0.68** | 1.25 | 0.89 | 0.96 |
| 8 | 0.00 | | 0.25 at My | 0.88 | 1.00 | 0.98 | 0.85 |
| 9 | 0.00 | | 0.00 | 1.04 | 0.83 | 0.85 | 1.01 |
| 10 | 0.00 | | 0.65 at My | 1.16 | 1.00 | 0.94 | 1.08 |
| 11 | 0.00 | | 0.00 | 1.04 | 0.78 | 0.80 | 0.91 |
| 12 | 0.00 | | 0.00 | 1.07 | 0.90 | 0.91 | 1.22 |
| 13 | 0.00 | | 0.00 | 0.87 | 0.84 | 0.84 | 0.88 |
| 14 | 0.00 | | 0.00 | 1.12 | 0.84 | 0.98 | 1.06 |
| 15 | 0.00 | | 0.10 at My | 0.8 | 0.90 | 0.88 | 0.91 |
| 16 | 0.00 | | 0.00 | **0.66** | 1.16 | 0.80 | 0.97 |
| 17 | 0.00 | | 0.00 | **0.59** | 0.97 | 0.78 | 0.77 |
| 18 | 0.00 | | 0.00 | 0.86 | 0.70 | 0.80 | 0.84 |
| 19 | 0.00 | | 0.00 | 0.75 | 0.82 | 0.86 | 0.83 |
| 20 | 0.00 | | 0.00 | 0.92 | 0.70 | 0.86 | 0.79 |
| 21 | 0.00 | | 0.00 | 1.01 | 0.66 | 0.77 | 0.93 |
| 22 | 0.25 | at My | 0.70 at My | 0.91 | 1.00 | 1.08 | 0.89 |
| 23 | 0.00 | | 0.20 at My | 0.87 | 0.86 | 0.99 | 0.81 |
| 24 | 0.00 | | 0.00 | 0.8 | 0.78 | 0.91 | 0.74 |
| 25 | 1.11 | at My | 0.75 at My | 0.73 | 1.22 | 1.23 | 0.81 |
| 26 | 0.22 | at My | 0.85 at My | 0.9 | 0.94 | 1.08 | 0.91 |
| 27 | 0.00 | | 0.45 at My | 0.86 | 0.92 | 1.00 | 0.80 |
| 28 | 1.70 | at My | 0.45 at My | 0.75 | 1.38 | 1.37 | 0.79 |
| 29 | 1.11 | at My | 0.90 at My | 0.84 | 1.19 | 1.23 | 0.93 |
| 30 | 0.25 | at My | 0.70 at My | 0.92 | 1.05 | 1.08 | 0.95 |
| 31 | 2.42 | at My | 1.85 at My | 0.91 | 1.85 | 1.60 | 1.03 |
| 32 | 1.82 | at My | 2.00 at My | 0.9 | 1.55 | 1.40 | 1.05 |
| 33 | 1.11 | at My | 0.95 at My | 0.85 | 1.30 | 1.23 | 0.96 |
| 34 | 3.23 | at My | 1.80 at My | 0.9 | 1.80 | 2.01 | 0.86 |
| 35 | 2.43 | at My | 1.70 at My | 0.81 | 2.00 | 1.60 | 0.87 |
| 36 | 1.70 | at My | 2.75 at My | 0.96 | 1.70 | 1.37 | 1.27 |
| 37 | 3.61 | at My | 2.50 at My | 0.94 | 2.20 | 2.25 | 0.92 |
| 38 | 3.25 | at My | 2.75 at My | 0.9 | 1.85 | 2.02 | 0.88 |
| 39 | 2.56 | at My | 1.85 at My | 0.95 | 1.75 | 1.65 | 0.87 |
| 40 | 4.20 | at Mp | 4.30 at Mp | 1.1 | 3.00 | 2.89 | 1.06 |
| 41 | 3.99 | at My | 3.15 at My | 0.94 | 2.40 | 2.78 | 0.94 |
| 42 | 3.28 | at My | 5.70 at My | 1.19 | 2.10 | 2.04 | 1.21 |
| | | | Mean = 0.91 | | | | 0.93 |
| | | | COV = 0.15 | | | | 0.13 |

## 3. Comparison of the experiments and the YLM model

### 3.1 Collapse curve

The hypothesis test is a statistical technique to establish whether two sets of measurements are significantly different. Using this technique, the collapse curves developed with the YLM model were compared with the experiment collapse curves. Significance is supported with the null hypothesis in which the mean values of the two sets of measurements are equal. In this case the matched pair *t*-test is applicable for normally distributed data (parametric tests). If the normality assumption has been violated for the experimental differences, the Wilcoxon signed-rank test as a non-parametric test procedure was used. All the collapse curves for the channel sections were tested with this technique and discrepancies were found to lie within the 95% confidence intervals. Accordingly it may be concluded that the experimental and YLM collapse curves are in good agreement.

### 3.2 Energy absorption

The total energy absorbed under large deformation pure bending of the channel sections was determined using the following equation

$$E = \int_0^{\theta} M d\theta \tag{54}$$

The integral represents the area under the moment-rotation curve, and the areas under the full large deformation moment-rotation curves (such as those shown in Fig. 7) were calculated, where the Simpsons rule was used for the curved portions. The total absorbed energy for the experimental and YLM results are compared in Table 2, where the YLM results are shown to compare relatively well, with a mean test/predicted ratio of 0.91 and COV of 0.15. In Fig. 8 the test/predicted ratio for the energy absorbed is compared with the width to depth ratio of the sections, where it is evident that as the width/depth ratio decreases the YLM model becomes increasingly unconservative.

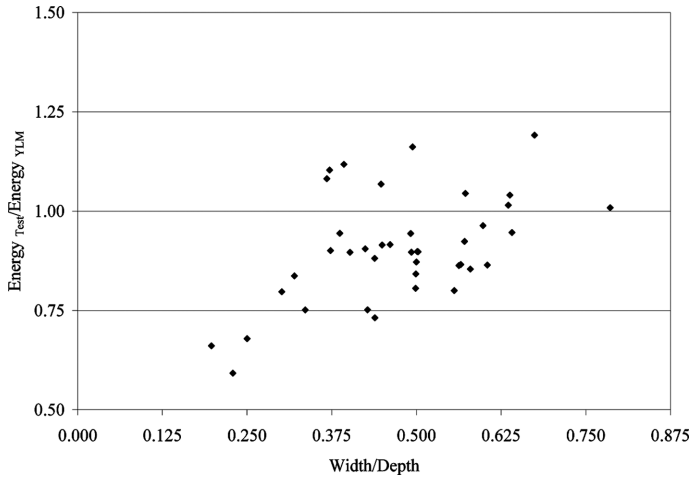


Fig. 8 Energy absorption from test results over the YLM results verses the width to depth ratio

## 4. Simplified YLM model

While the collapse curve of the YLM solution compares well with the experimental results, the geometry and the determination of the work done by the various hinge lines are complex, and provide significant computational complexity to analysts wishing to describe the full bending moment-rotation behaviour of channel sections. In order to reduce this complexity, a simplified empirical formula was determined. From the YLM analysis it was determined that for the collapse curve the normalised moment is a function of the normalised curvature, given by the generalised Eq. (55)

$$M/Mp = X(k/k_p)^{-0.665} \tag{55}$$

where $k_p$ is the sections plastic curvature.

The exponent −0.665 was determined from trial and error, and values of the constant $X$ were then similarly determined. An example curve fitting is shown in Fig. 9, where $X$ was found to be 1.0 in order for the curve to closely match the experimental curve. Values of $X$ for all sections are tabulated in Table 2.

In order to generalise Eq. (55) further, for any channel section geometry, an equation for the constant $X$ was sought as a function of the slenderness ratio ($\lambda$). Plotting $X$ as a function of the slenderness non-dimensionalised to the plastic slenderness, revealed the trend shown in Fig. 10, from which the generalised Eq. (56) was developed

$$\frac{M}{M_p} = 2.8\left(\frac{\lambda_s}{\lambda_p}\right)^{-0.665}\left(\frac{k}{k_p}\right)^{-0.665} \tag{56}$$

The coefficient 2.8 was found to be the best fit for the test curves. The values of the constant $X$ determined from Eq. (56) are compared with those determined from the experiments in Table 2. In Fig. 11 sample experimental curves are compared with the simplified YLM for a non-compact and compact section.

Calculating the total energy absorbed under large deformation pure bending of the channel sections for the simplified YLM, according to the method outlined in section 3.2, yields the results

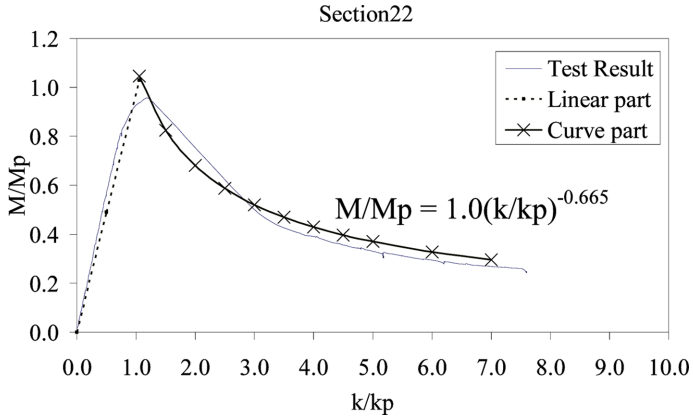


Fig. 9 Curve fitting Eq. (55) with the experimental results

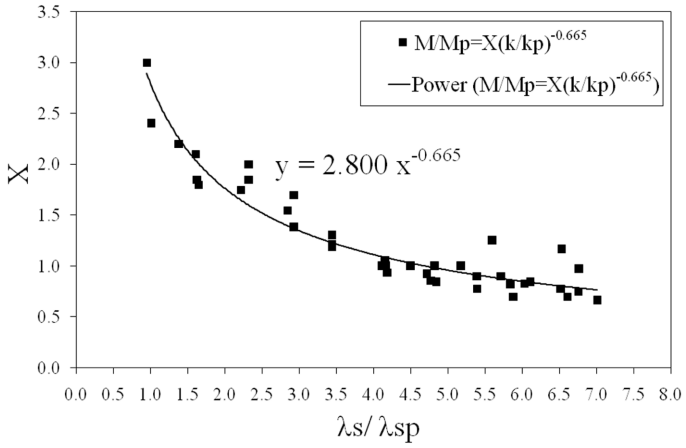


Fig. 10 The best curve fit for calculating the constant $X$ from the ratio of the sections slenderness to the plastic slenderness limit

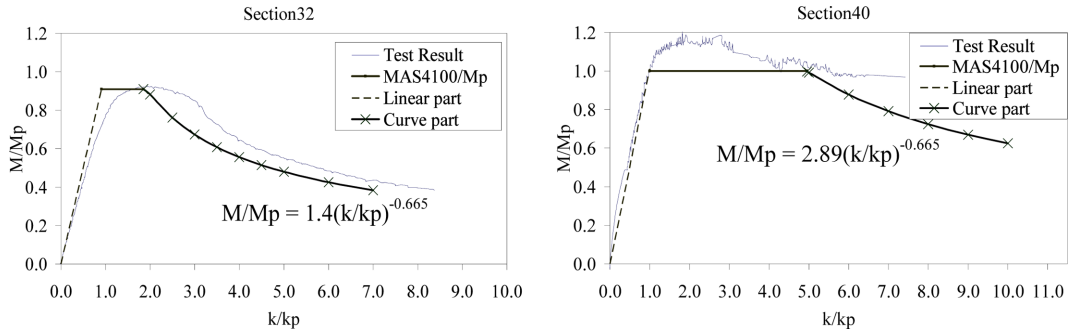


Fig. 11 Normalised moment-curvature diagram from the experiments compared with the simplified proposed method for (a) non-compact and (b) compact sections

tabulated in Table 2. The test/predicted values are in close agreement with those using the exact collapse curve, with a mean of 0.93 and COV of 0.13. These results indicate that the simplified YLM produces accurate and reliable determinations of the energy absorbed by cold-formed channel sections under large deformation major-axis pure bending.

## 5. Conclusions

A theoretical procedure has been developed to determine the large deformation bending moment-rotation behaviour of cold-formed steel channel sections with flange edge stiffeners under major-axis bending. Theoretical plastic collapse curves were developed with yield line mechanism theory using the energy method, and were used in conjunction with an in-plane plastic theory to model the full moment-rotation response. The in-plane rotation capacity of non-slender sections was determined with an empirical estimation based on the section slenderness value. Both the collapse curves and energy absorbed under large deformation bending were shown to compare well with the

results of 40 experiments of cold-formed steel channel sections with a variety of section geometries, and with simple or complex flange edge stiffeners. Due to the inherent complexities of the geometry and work equations for the yield lines in the spatial plastic mechanism, a simplified equation to represent the plastic collapse curve was additionally developed, and was shown to provide accurate and reliable determinations of the energy absorbed by cold-formed channel sections under large deformation major-axis pure bending.

## References


AS 4100 (1998), *Australian Standard*, Steel Structures, Standards Australia, Sydney.

Bambach, M.R., Tan, G. and Grzebieta, R.H. (2009), "Steel spot-welded hat sections with perforations subjected to large deformation pure bending", *Thin Wall. Struct.*, **47**(11), 1305-1315.

Cimpoeru, S.J. (1992), "The modelling of the collapse during roll-over of bus frames consisting of square thin-walled tubes", Doctor of Philosophy, Civil Engineering, Monash University.

Davies, P., Kemp, K.O. and Walker, A.C. (1975), "Analysis of the failure mechanism of an axially loaded simply supported steel plate", *Proceedings of the Institution of Civil Engineers (London), Part 1 - Design & Construction*, **59**(2), 645-658.

Elchalakani, M. (2007), "Plastic mechanism analyses of circular tubular members under cyclic loading Source", *Thin Wall. Struct.*, **45**(12), 1044-1057.

Kecman, D. (1983), "Bending collapse of rectangular and square section tubes", *Int. J. Mech. Sci.,* **25**(9-10), 623-636.

Kotelko, M. (1996), "Ultimate load and post failure behaviour of box-section beams under pure bending", *Eng. Trans.*, **44**(2), 229-251.

Kotelko, M. (2007), "Load-carrying capacity and energy absorption of thin-walled profiles with edge stiffeners", *Thin Wall. Struct.*, **45**(10-11), 872-876.

Maduliat, S., Bambach, M.R. and Zhao, X.L. (2012), "Inelastic behaviour and design of cold-formed channel sections in bending", *Thin Wall. Struct.*, **51**, 158-166.

Murray, N.W. and Khoo, P.S. (1981), "Some basic plastic mechanisms in the local buckling of thin-walled steel structures", *Int. J. Mech. Sci.,* **23**(12), 703-713.

Murray, N.W. (1984), "The effect of shear and normal stress on the plastic moment capacity on inclined hinges in thin-walled steel structures", *Festschrift Roik, Inst. fur Konstruktiven Ingenieurbau, Ruhr Univ. Bochum,* **84**, 237-248.

Nagel, G. (2005), "Impact and energy absorption of straight and tapered rectangular tubes", Doctor of Philosophy, *Built Environment & Engineering, Queensland University of Technology.*

Setiyono, H. (2007), "Plastic mechanism and elastic-analytical approaches applied to estimate the strength of an axially compressed-thin-walled channel steel section beam", *Int. J. Mech. Sci.*, **49**(3), 257-266.

Tan, G. (2009), "Perforated hat sections subjected to large rotation pure bending", Master of Engineering Science, Civil Engineering, Monash University.

Ungureanu, V., Kotelko, M., Mania, R.J. and Dubina, D. (2010), "Plastic mechanisms database for thin-walled cold-formed steel members in compression and bending", *Thin Wall. Struct.*, **48**(10-11), 818-826.

Ye, J.H., Zhao, X.L., Van, B.D. and A-Mahaidi, R. (2007), "Plastic mechanism analysis of fabricated square and triangular sections under axial compression", *Thin Wall. Struct.*, **45**(2), 135-148.

Zhao, X.L. and Hancock, G.J. (1993), "Experimental verification of the theory of plastic-moment capacity of an inclined yield line under axial force", *Thin Wall. Struct.*, **15**(3), 209-233.

Zhao, X.L. and Hancock, G.J. (1993a), "A theoretical analysis of the plastic-moment capacity of an inclined yield line under axial force", *Thin Wall. Struct.*, **15**(3), 185-207.

Zhao, X.L. (2003), "Yield Line Mechanism Analysis of Steel Members and Connections", *Prog. Struct. Eng. Mater.*, **5**(4), 252-262.